Novel elastic deformation mechanism in multifunctional Ti–Nb alloy

Zhaowei Zhu[a], Yandong Wang[a,*], Yulin Hao[b], Jiapeng Liu[c], Qinghua Zhang[c], Runguang Li[a], Haoliang Wang[b], Yang Ren[d]

[a] State Key Laboratory for Advanced Metals and Materials, University of Science and Technology Beijing, Beijing 100083, PR China

[b] Shenyang National Laboratory for Materials Science, Institute of Metal Research, Chinese Academy of Science, Shenyang 110016, PR China

[c] School of Materials Science and Engineering, Beijing Institute of Technology, Beijing 100081, PR China

[d] X-ray Science Division, Argonne National Laboratory, Argonne, IL 60439, USA

E-mail addresses: ydwang@ustb.edu.cn (Y.D. Wang).

Abstract

In-situ high-energy X-ray diffraction was used to reveal a novel elastic deformation mechanism of the polycrystalline Ti-24Nb-4Zr-8Sn alloy under uniaxial compression. These experiments of polycrystal provide direct evidence on anomalous change in full widths at half maximum for $\{110\}_\beta$ peak during elastic deformation, i.e. peak broadening during unloading and peak narrowing upon loading, which is attributed to the formation of stress-induced irreversible ω phase as clearly demonstrated in single crystal during compression. Difference in modulus between ω and β phases induces different change in lattice strain causing the broadening and narrowing of diffraction peak near $\{110\}_\beta$ where actually contains $\{1120\}_\omega$ under different applied stress. This study offers new perspectives to investigate intrinsic mechanism on specific phase transformation during elastic deformation.

Key words: Titanium alloys; High-energy X-ray diffraction; Compression test; Elastic

behavior

1. Introduction

Several mechanisms have been proposed to explain the anomalous deformation behavior of multifunctional gum metals [1] which include the formation of the nano-disturbances [2], the deformation twinning [3], the reversible stress-induced martensitic transformation [4], and the spatially confined martensitic transformation from BCC structure to α" and δ phases [5,6]. The Ti-24Nb-4Zr-8Sn alloy (abbreviated as Ti2448), a kind of gum-like metal, has been investigated in early works [5-7]. Previous investigations have been focused on the peculiar properties during tensile deformation to clarify the possible physical mechanisms [3-7]. However, the underlying physical mechanisms responsible for compression of the Ti2448 alloy that exhibits pronounced tension-to-compression asymmetry still remain elusive. Herein we use the in-situ synchrotron-based high-energy X-ray (HE-XRD) diffraction to investigate the deformation behavior of the polycrystalline Ti2448 alloy under compression. Our present investiga- tions are intended to clarify the detailed cyclic compression process, which would allow us to understand the anomalous elastic deformation behavior of the Ti2448 alloy.

2. Materials and experimental methods

Ingot with composition of Ti-24Nb-4Zr-8Sn alloy (in mass%) was processed by arc-melting and hot forged at 1123 K into 55 mm in diameter and then hot rolled to 12 mm in diameter at 1072 K. Single crystal was grown in an optical floating-zone furnace

(FZ-T-12000-X- VP-S, Crystal System Inc.) under protection of flowing argon. Uniaxial compression tests were conducted in ambient air at room temperature using specimens with a rectangular cross-section of 2×2 mm and length of 4 mm at a strain rate of 1.3×10^{-4} s^{-1}. The in-situ synchro- tron-based HE-XRD experiments were conducted on the 11-ID-C beamline at the Advanced Photon Source, Argonne National Laboratory [8]. The size of X-ray beam is 0.5×0.5 mm^2 with energy of 115 keV (wavelength ~0.10798 Å). The X-ray two-dimensional diffraction images were processed by Fit2D image processing software.

3. Results and discussion

The nominal uniaxial cyclic compression stress-strain (S-S) curves for polycrystalline Ti2448 alloy which is a single β phase with BCC structure tested at room temperature are shown in Fig. 1(a). The first and second elastic cyclic compression curves display almost linear deformation with the Young's modulus of ~50 GPa. The engineering strains of the first and second cycles are almost fully recovered. Plastic deformation occurred when the stress was increased to the compres- sion yield strength (~570 MPa) in the third cycle. Lattice strain-stress curves for $\{110\}_\beta$, $\{200\}_\beta$ and $\{211\}_\beta$ planes along loading direction (LD) under cyclic deformation mode are demonstrated in Fig. 1(b–d). The structure evolution can be clearly understood from the change in lattice strains (hkl), i.e. $\varepsilon_{hkl}=(d_{hkl}-d_0)/d_0$, where d_0 and d_{hkl} correspond to the interplanar spacing for different (hkl) crystalline planes without and with an external stress, respectively. The diffraction elastic moduli determined from the slope of the

lattice strain-stress curves in the linear region up to a stress applied at ~250 MPa remain almost constant, which are 45 GPa, 43 GPa, and 47 GPa for the $\{110\}_\beta$, $\{200\}_\beta$ and $\{211\}_\beta$ planes, respectively, as shown in Fig. 1(b). The almost same values for diffraction elastic moduli observed in the above mentioned crystalline planes indicate that the studied polycrystalline alloy exhibits an isotropic elasticity.

However, when the applied stress exceeds 450 MPa (slightly smaller than the yield strength of ~570 MPa), non-linear lattice strains as a function of applied stress are evidenced for $\{110\}_\beta$ and $\{200\}_\beta$ planes, as shown in Fig. 1(c) and (d). The diffraction elastic modulus of $\{211\}_\beta$ plane remains constant, but $\{110\}_\beta$ and $\{200\}_\beta$ planes show moduli stiffening and softening, respectively (Fig. 1(c)). After unload-ing for the second and third cycles, the lattice strain of the $\{211\}_\beta$ remains unchanged, while the lattice strains of $\{110\}_\beta$ becomes tensile and $\{200\}_\beta$ becomes compressive.

The evolution of FWHMs for the $\{110\}_\beta$, $\{200\}_\beta$ and $\{211\}_\beta$ peaks of polycrystalline Ti2448 alloy, which provide further understanding of deformation mechanisms, are shown in Fig. 2(a–c). Reversible broadening for $\{200\}_\beta$ and $\{211\}_\beta$ diffraction peak can be observed during the first two cycles, as shown in Fig. 2(a–b). In the third cycle, FWHMs of $\{200\}_\beta$ and $\{211\}_\beta$ peaks increase rapidly and faster than $\{110\}_\beta$ when the applied stress exceeds the yield strength (~570 MPa). Unloading induced a decrease in FWHMs for $\{211\}_\beta$ and a plateau for $\{200\}_\beta$. Interestingly, the FWHM for $\{110\}_\beta$ diffraction peak increases during loading and still continuously raise during unloading in the second and third cycles, which is totally different from that

observed for $\{200\}_\beta$ and $\{211\}_\beta$ diffraction peaks. And peak narrowing can be found during loading of the third cycle when the stress increases to 300 MPa. The FWHM curves for the unloading of the second cycle and the loading of the third cycle are almost overlapping, as detailed shown in Fig. 2(d). The anomalous change in FWHM, i.e. peak broadening during unloading and peak narrowing upon loading, for $\{110\}_\beta$ diffraction peak during elastic deformation is firstly reported so far.

In-situ HE-XRD compressive experiments were performed on ⟨110⟩ oriented Ti2448 single crystal (with the X-ray beam along $[001]_\beta$ zone axis and LD along $[110]_\beta$), as shown in Fig. 3, to perceive the above-mentioned anomalous elastic deformation mechanism. For the virgin single crystal, the primary diffraction spots originate from β phase with BCC structure and weak diffuse scattering signals are attributed to small amount of nano-sized domains (NDs) of α" martensite [9] (indicated by red circle in Fig. 3(a)). While the applied stress exceeds ~478 MPa, ω phase starts to form and α" martensite vanishes (Fig. 3(b)). Furthermore, the newly formed ω phase still remains after unloading (Fig. 3(c)). In fact, ω phase is coherent with β phase, obeying a crystallographic relationship described as $(0001)_\omega//(111)_\beta$, $[1120]_\omega//[011]_\beta$ [10]. Based on the calculation by the PowderCell software, the diffraction profiles of $\{110\}_\beta$ and $\{1120\}_\omega$ are given in Fig. 3(d), which indicates that two diffraction peaks are very close.

Peak broadening of X-ray diffraction can be attributed to two reasons, i.e. the decrease in coherent scattering volume and the presence of inhomogeneous strain field [11]. Possible physical source of inhomogeneous strain may be due to the existence of

crystal defects, micro-stresses [12], but other sources such as elastic anisotropy [13] could also contribute to the peak broadening. In our case, loading induced reversible diffraction peak broadening with a similar phenomenon reported in nanocrystalline nickel [11]. Our previous investigations on the $Ni_{43}Fe_{18}Ga_{27}Co_{12}$ single crystal suggest that heterogeneous strain field originates from the fluctuation in elastic strain due to the formation of the nano-domains of martensite (i.e. confined martensite), which contributes to the reversible peak broadening during elastic deformation [13]. Based on the in-situ deformation study of Ti2448 single crystal alloy, the anomalous change in FWHMs is closely related to the deformation-induced irreversible ω phase. For our studied case in polycrystalline Ti2448 alloy, similar to that found in $Ni_{43}Fe_{18}Ga_{27}Co_{12}$ single crystal, the peak broadening for three diffraction planes during loading in the elastic region originates from an increase in elastic strain heterogeneity inside β phase due to deformation-induced confined ω phase. The microstresses, generated due to the formation of ω phase and the complex interaction between ω and β phases, lead to the additional heterogeneity strain during the cycle unloading. Due to the crystallographic orientation relationship between ω and β phases, i.e. $(0001)_\omega//(111)_\beta$ and $[1120]_\omega//[011]_\beta$, the diffraction peak near $\{110\}_\beta$ actually contains $\{1120\}_\omega$. The difference in modulus between ω and β phases induces different change in lattice strain causing the broadening and narrowing of diffraction peak near $\{110\}_\beta$ under different applied stress. When the stress exceeds yield strength, increase in density of dislocations attributes to continuously peak broadening for three planes. The smaller increase of FWHM for

$\{110\}_\beta$ is probably due to lower dislocations density as the modulus stiffening.

4. Conclusion

The in-situ synchrotron-based HE-XRD diffraction experiments were employed to reveal the novel elastic deformation mechanism of polycrystalline Ti2448 alloy under cyclic uniaxial compression. The anomalous change in FWHM for $\{110\}_\beta$ peak during elastic deformation is found. The observed novel elastic behavior is attributed to the interaction between the newly formed ω phase and matrix with BCC structure. Our finding on new elastic compression mechanism in the gum-type alloy would provide an in-depth understanding of the specific phase transformation related elastic deformation mechanism.

Acknowledgement

This work was supported by National Natural Science Foundation of China (NSFC) (Grant no.s 51471032 and 51527801), the National Basic Research Program of China (973 Program) under Contract no. 2012CB619405, the Fundamental Research Funds for the Central Universities (Grant no. 06111020), and the fundamental research fund at the State Key Laboratory for Advanced Metals and Materials (2016Z-01, 2016Z-12, 2016Z-19). This research used resources of the Advanced Photon Source, a U.S. Department of Energy (DOE) Office of Science User Facility operated for the DOE Office of Science by Argonne National Laboratory under Contract No. DE-AC02-06CH11357.

References

[1] T. Saito, T. Furuta, J.H. Hwang, S. Kuramoto, K. Nishino, N. Suzuki, et al., Science 300 (2003) 464-467.

[2] M.Y. Gutkin, T. Ishizaki, S. Kuramoto, I.A. Ovid'ko, Acta Mater. 54 (2006) 2489-2499.

[3] H. Xing, J. Sun, Appl. Phys. Lett. 93 (2008) 031908.

[4] J.W. Morris Jr, Y. Hanlumyuang, M. Sherburne, E. Withey, D.C. Chrzan, S. Kuramoto, et al., Acta Mater. 58 (2010) 3271-3280.

[5] J.P. Liu, Y.D. Wang, Y.L. Hao, Y.Z. Wang, Z.H. Nie, D. Wang, et al., Sci. Rep. 3 (2013) 2156.

[6] J.P. Liu, Y.D. Wang, Y.L. Hao, H.L. Wang, Y. Wang, Z.H. Nie, et al., Acta Mater. 81 (2014) 476-486.

[7] Y.L. Hao, H.L. Wang, T. Li, J.M. Cairney, A.V. Ceguerra, Y.D. Wang, et al., J. Mater. Sci. Technol. 32 (2016) 705-709.

[8] T.K. Liu, G.L. Wu, C.K. Liu, Z.H. Nie, T. Ungár, Y. Ren, Mater. Sci. Eng. A 568 (2013) 83-87.

[9] M. Tahara, H.Y. Kim, T. Inamura, H. Hosoda, S. Miyazaki, Acta Mater. 59 (2011) 6208-6218.

[10] J. Šmilauerová, P. Harcuba, D. Kriegner, M. Janeček, V. Holý, Acta Mater. 100 (2015) 126-134.

[11] Z. Budrovic, H.V. Swygenhoven, P.M. Derlet, S.V. Petegem, B. Schmitt, Science

304 (2004) 273-276.

[12] T. Ungár, Scr. Mater. 51 (2004) 777-781.

[13] Q.H. Zhang, Z. Zhai, Z.H. Nie, S. Harjo, D.Y. Cong, M.G. Wang, et al., J. Appl. Crystallogr. 48 (2015) 5034.

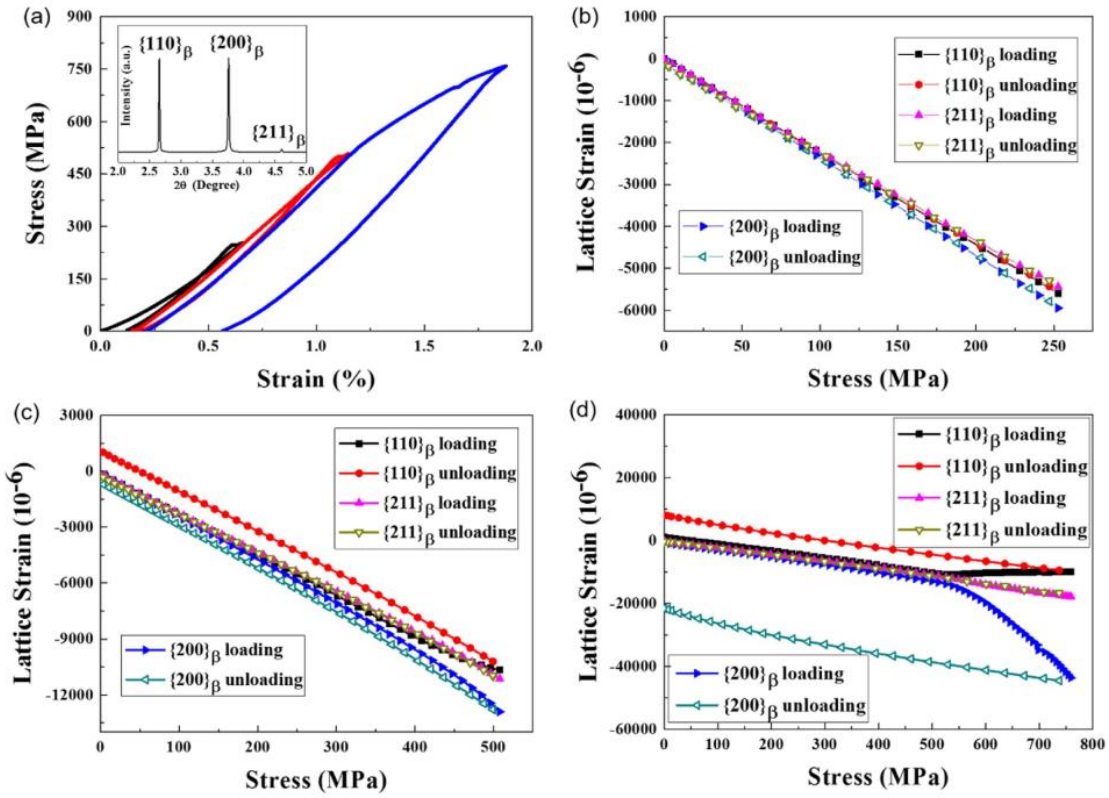

Figure 1. The nominal uniaxial cyclic compression stress-strain (S-S) curves of polycrystalline Ti2448 alloy at room temperature (a). The inset in (a) is 1-dimensional HE-XRD profile of Ti2448 alloy before compression. The lattice strain-stress curves for $\{110\}_\beta$, $\{200\}_\beta$ and $\{211\}_\beta$ planes: the first cycle (b), the second cycle (c), the third cycle (d).

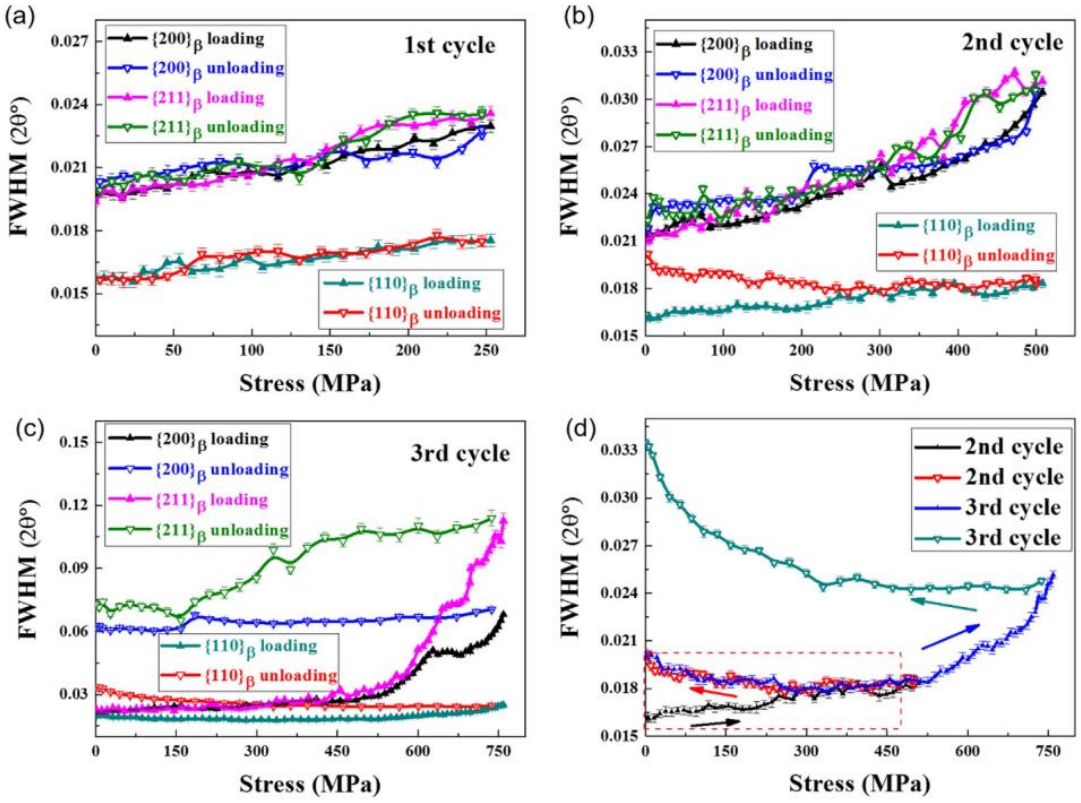

Figure 2. Fig. 2. The change in FWHMs for $\{200\}_\beta$, $\{110\}_\beta$ and $\{211\}_\beta$ peaks of polycrystalline Ti2448 alloy as a function of uniaxial cyclic compression: the first cycle (a), the second cycle (b), the third cycle (c). The highlighted change in FWHM for $\{110\}_\beta$ peak for the second and third cycles (d).

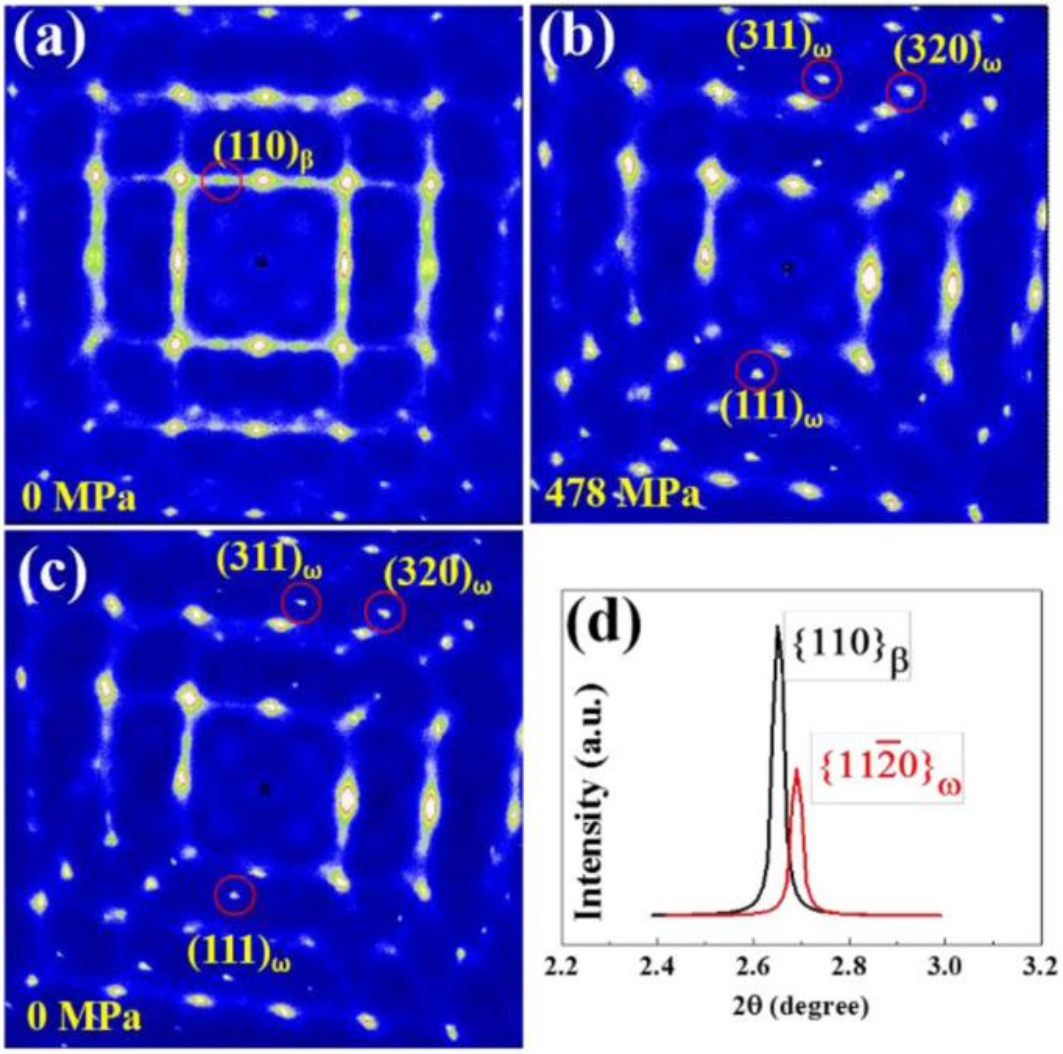

Fig. 3. The HE-XRD patterns for ⟨110⟩ oriented Ti2448 single crystal with the beam along $[001]_{\beta}$ zone axis under compression mode: before deformation (0 MPa) (a), loaded at 478 MPa (b), unloaded at 0 MPa (c), The diffraction profiles of $\{110\}_{\beta}$ and $\{1120\}_{\omega}$ (d).